JHEP PROCEEDINGS

Heavy Flavours 8, Southampton, UK, 1999

Onium and b Production at the Tevatron

K. Sumorok

MIT , 77 Massachusetts Ave, Cambridge MA 02139 USA
E-mail: Sumorok@mitlns.mit.edu

Abstract: Recent data from the CDF and D0 experiments at the Tevatron are presented on b quark production cross sections, J/ψ, ψ' and Υ production cross sections. An analysis from CDF of the production polarization of the J/ψ, ψ' and $\Upsilon(1S)$ is reviewed and the results discussed in the context of the color octet model.

1. Introduction

The Tevatron is a copious source for b quark production compared with e^+e^- colliders and provides many tests of both perturbative and non-perturbative QCD. Recent experimental results on the b quark production cross section at the Tevatron by D0 are presented in section 2 and compared with a NLO QCD prediction.

In section 3 we summarise recently published results using 17.8 pb^{-1} of data from CDF on J/ψ and ψ' production where prompt production and B decay production have been separated. In the case of J/ψ the contribution to the prompt production from χ_c and ψ' is also extracted to give the direct production cross section. This direct J/ψ production and the prompt ψ' production are found to be "anomalously" high by a factor of 50 compared with the color singlet model. A possible explanation in terms of the color octet model is discussed. A consequence of this model is transversely polarized ψ's at high P_T^{ψ}.

In section 4 using 110 pb^{-1} of dimuon trigger data, a recent analysis by CDF on the production polarization of the J/ψ is presented and in section 5 results from a similar analysis are given on the ψ'. In section 6 using 77 pb^{-1} of data, new results from CDF on the $\Upsilon(1S)$, $\Upsilon(2S)$ and $\Upsilon(3S)$ differential cross sections are given and a measurement of the fraction of directly produced $\Upsilon(1S)$ presented. An analysis of the production polarization of the $\Upsilon(1S)$ measured by CDF is also presented.

2. b quark production cross sections

The b quark production cross section has been measured at the Tevatron by both CDF [1] and D0 [2] and found to be a factor of ∼2.5 larger than the NLO theoretical predictions of NDE [3] and MNR [4]. D0 has a new measurement of the $b\bar{b}$ production cross section at 1.8 TeV based on the observation of 2 jets each with an associated muon.

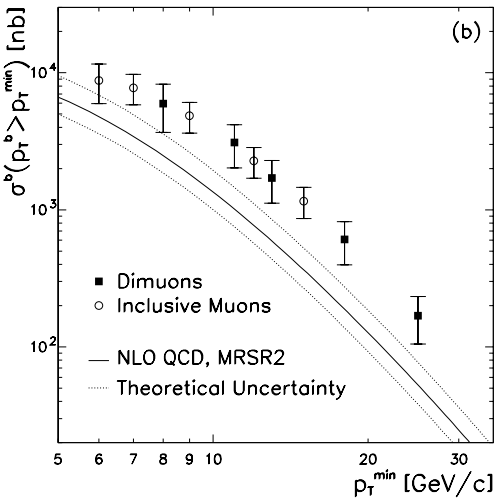

Figure 1: b quark production cross section and the NLO QCD prediction

Figure 1 shows the b quark production cross section from these dimuon data and previously published data from inclusive muons along with the NLO QCD prediction. As with previous mea-

surements the theory curve lies significantly below the data. By measuring both b and $\bar{b}$ in an event it is possible to look at the angular correlation between the two muons and compare that with theory. Figure 2 shows the angular distribution $\Delta\phi^{\mu\mu}$ for the two muons compared with the theory. Again the data show an excess above the NLO calculation but the shape is well reproduced. The LO prediction does not describe the data. This measurement complements previous published angular correlations in $b\bar{b}$ jets [5] and μ-jet [6] distributions by the UA1 and CDF experiments respectively.

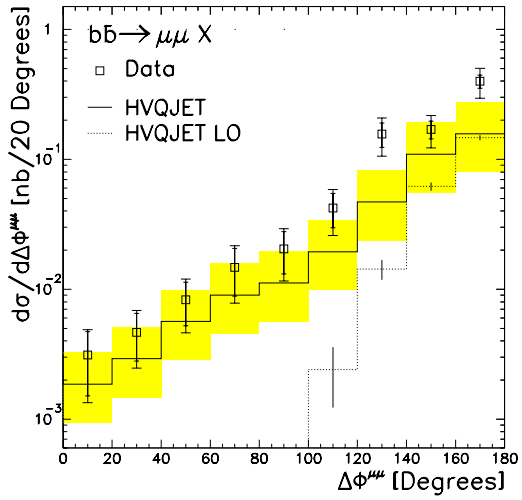

Figure 2: The $\Delta\phi^{\mu\mu}$ spectrum for $b\bar{b}$ production compared to the NLO prediction (solid histogram) with the theoretical uncertainty (shaded area). Also shown is the LO prediction (dotted histogram).

3. J/ψ and ψ' Production

Measurements of the J/ψ and ψ' differential cross sections by CDF [7] separate the cross sections into those ψ mesons coming from b flavoured hadron production from those originating from a prompt production mechanism. This separation is made by reconstructing the decay vertex of the J/ψ and ψ' using the Silicon Vertex (SVX) detector of CDF. The fraction of J/ψ coming from b flavored hadron production was found to increase from 15% at 5 GeV/c up to near 40% at 18 GeV/c $P_T^{J/\psi}$. For ψ', a similar increase is seen in the range from 5 to 14 GeV/c $P_T^{\psi'}$.

Figure 3 compares the differential cross sections of J/ψ and ψ' coming from B hadron decays with the NLO QCD calculation [3]. The b flavored hadron production differential cross sections are found to be higher than the theoretical prediction, for central value parameters, by a factor of approximately 2 to 4.

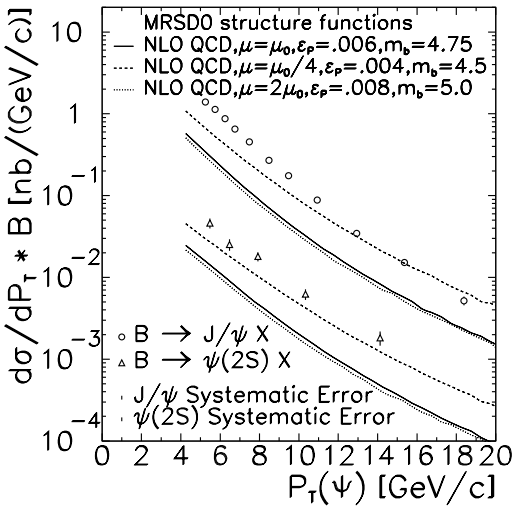

Figure 3: The differential cross section times branching ratio $B(\psi \to \mu^+\mu^-)$ for ψ mesons from b hadron decays

Figure 4 compares the differential cross sections of prompt J/ψ and ψ' and the theoretical predictions based on the color singlet model (CSM) [8]. The measured prompt production cross sections are also higher than the theoretical predictions based on the CSM by factors of ≈ 6 for J/ψ and ≈ 50 for the ψ' respectively.

The prompt production for J/ψ has three components, namely a feed-down from χ_c production, a feed-down from ψ' and a pure direct component as in the ψ' production. CDF has measured the prompt J/ψ rate coming from χ_c production to be $(29.7 \pm 1.7 \pm 5.7)\%$ of the total prompt production [9]. This measurement is

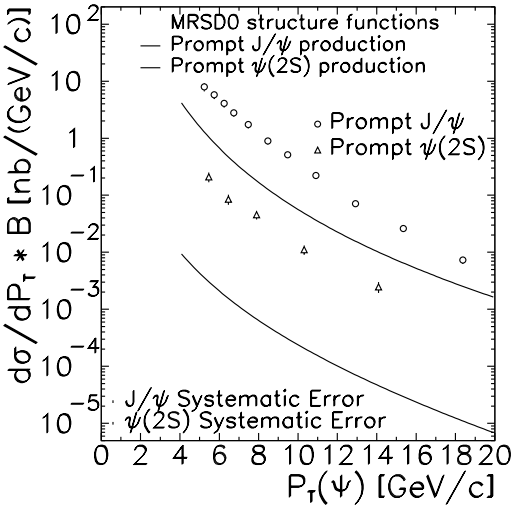

Figure 4: The differential cross section times branching ratio $B(\psi \to \mu^+\mu^-)$ for prompt ψ mesons

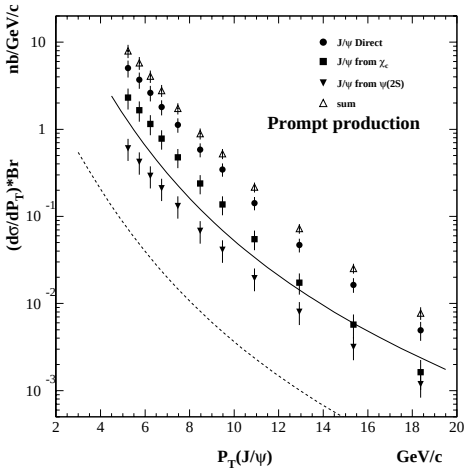

Figure 5: The differential cross sections of prompt $J/\psi \to \mu^+\mu^-$ as a function of $P_T^{J/\psi}$. The dashed curve is the CSM calculation for J/ψ production and solid curve is the calculation of $\chi_c \to J/\psi\gamma$

made by looking for photon candidates above 1 GeV in association with the $J/\psi \to \mu^+\mu^-$ decays and then looking at mass difference $\Delta M = M(\mu^+\mu^-\gamma) - M(\mu^+\mu^-)$. From the measured ψ' production cross section the fraction of the prompt J/ψ's feeding down from ψ' decays is calculated to be $7 \pm 2\%$ at $P_T^{J/\psi} = 5$ GeV/c to $15 \pm 5\%$ at $P_T^{J/\psi} = 18$ GeV/c. The fraction of directly produced J/ψ's is $64 \pm 6\%$ and is approximately independent of $P_T^{J/\psi}$ between 5 and 18 GeV/c. Figure 5 shows the differential cross section of prompt J/ψ production including the different components.

Having separated out the the prompt J/ψ coming from χ_c, both the direct prompt J/ψ and the ψ' production appear to be ≈ 50 times higher than CSM predictions. The solid curve in Figure 5 is the calculation for $\chi_c \to J/\psi\gamma$ which includes contributions from the CSM and the Color Octet Model (COM) [10] and tends to be below the J/ψ data coming from χ_c at lower $P_T^{J/\psi}$.

One of the theoretical models which tries to explain this anomalous production is the COM [11]. The model raises the prompt production cross section by including color-octet $c\bar{c}$ states in the fragmentation process. Figure 6 shows the differential cross section for $\psi' \to \mu^+\mu^-$ fitted to these production mechanisms. The singlet term has a $1/P_T^8$ dependence, the terms ${}^1S_0^{(8)}$ and ${}^3P_0^{(8)}$ a $1/P_T^6$ dependence and the ${}^3S_1^{(8)}$ term a $1/P_T^4$. This latter term, which fragments from a single gluon in production, is seen to dominate at high P_T. A single gluon is transverely polarized and it is predicted that this polarization is transfered to the J/ψ or ψ'.

A consequence of this mechanism is that the direct prompt J/ψ and the ψ' will approach 100% transverse polarization at leading order in α_s and transverse momenta P_T for $P_T^2 \gg m_c^2$ where m_c is the charm quark mass [12]. Observation of such a polarization would therefore be an indication of the color-octet fragmentation mechanism. In addition, knowledge of the polarization would help decrease the systematic uncertainties on the acceptance of ψ decays hence improving the measurement of cross sections.

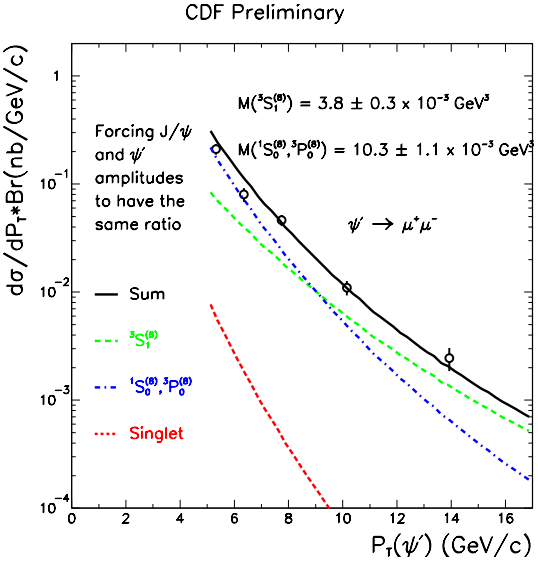

Figure 6: Fitted COM prediction to the differential cross section for $\psi' \to \mu^+\mu^-$

4. Measurement of Production Polarization of J/ψ

For this study CDF uses the Run I data sample corresponding to 110 pb^{-1} integrated luminosity. Events were selected with dimuon triggers. The dimuon mass plot (not shown), exhibits a clear J/ψ peak with a signal to background ratio (S/B) of approximately 20 and a mass resolution varying from 15 MeV/c^2 at 4 GeV/c $P_T^{J/\psi}$ to 30 MeV/c^2 at 20 GeV/c $P_T^{J/\psi}$. Figure 7 shows the helicity basis frame in which the z axis is defined as along the J/ψ direction in the overall center of mass (Lab. frame) and the y axis is the production plane normal. The angle θ is given by the direction of the μ^+ with respect to the J/ψ direction in the J/ψ center of mass frame. The normalized angular distribution $I(\theta)$ is given by

$$I(\theta) = \frac{3}{2(\alpha+3)}(1+\alpha\cos^2\theta). \qquad (4.1)$$

Unpolarized J/ψ would have $\alpha = 0$ whereas $\alpha =$ 1 and -1 correspond to fully transverse and longitudinal polarizations respectively. Experimentally the angular distribution $I(\theta)$ is severely cut by the acceptance as $|cos\theta|$ approaches 1.0 due to the P_T cut on the muons in the Lab. frame. The value of α is extracted by a χ^2 fitting method whereby Monte Carlo dimuon events are generated and passed though the experimental acceptance and compared with the background subtracted angular distribution.

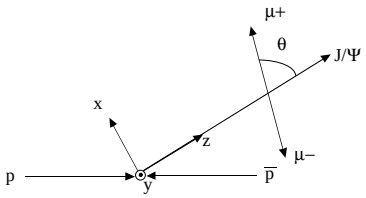

Figure 7: Sketch showing the coordinate system in the helicity frame.

In order to extract the polarization parameter for prompt J/ψ production, we need to separate the prompt component from the B decay component. The proper decay length, ct, is related to the J/ψ decay length L_{xy} as follows:

$$ct = \frac{M_{J/\psi}L_{xy}}{F_c P_T^{J/\psi}} \qquad (4.2)$$

where $M_{J/\psi}$ is the reconstructed J/ψ mass. The decay length L_{xy} is measured in the transverse plane of the CDF detector with the SVX. The factor $F_c = 2.44xe^{-1.18P_T^{J/\psi}} + 0.84$ is an average correction factor obtained from Monte Carlo studies to account for the fact that we use the J/ψ P_T instead of the B P_T.

Figure 8 shows the fitted ct distribution of the J/ψ's to get the relative fractions of pure prompt and B decay in different ct bins. The total B decay fraction is also measured. Dividing the data into short and long lived regions it can be seen that the prompt decays dominate the short-lived region and the B decays dominate the long-lived region. For extracting α, the data are divided into 7 P_T and 3 subsamples; SVX short-lived $-0.1 \leq ct \leq 0.013$ cm; SVX long-lived $0.013 \leq ct \leq 0.3$ cm and CTC (Central Tracking Chamber) where the SVX information on the muons was missing. In each subsample

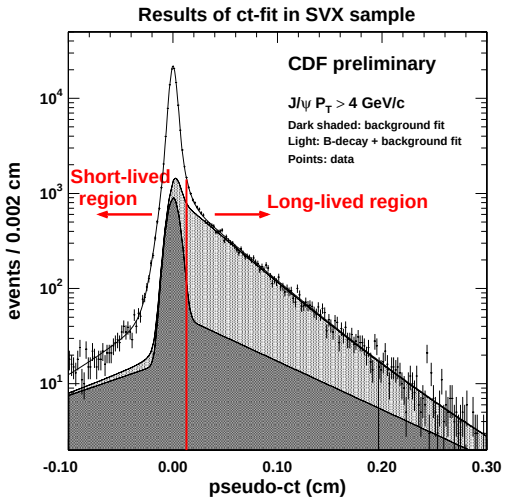

Figure 8: Measured *ct* distribution of J/ψ's showing the fitted prompt and B decay components

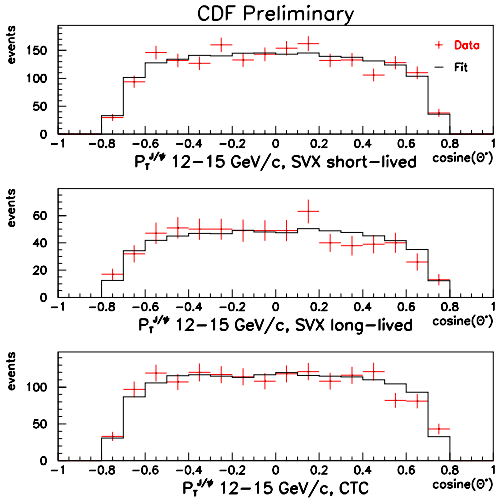

Figure 9: Example of fitted *cosθ* distributions in the $P_T^{J/\psi}$ 12-15 GeV/c bin

the *cosθ* distribution was fitted to a sum of 2 angular distributions, (equation 4.1), with parameters α^P and α^B corresponding to prompt and B decay production respectively. The relative fraction of each distribution was known from the fits to the *ct* distributions and in the case of the CTC subsample the total fitted B fraction from the *ct* fits was used. Figure 9 shows an example of fitted *cosθ* distributions in the $P_T^{J/\psi}$ 12-15 GeV/c bin. The effect of the acceptance on the angular distribution is clearly seen.

Figure 10 shows the fitted values of α^P and α^B as a function of $P_T^{J/\psi}$ in the range 4 to 20 GeV/c. The error bars include estimates of the systematic errors which in general are small compared with statistical errors. The prompt polarization α^P is seen to rise above 6 GeV/c $P_T^{J/\psi}$ but is then seen to fall so that at high $P_T^{J/\psi}$ it is consistent with zero. The value of α^B is consistant with zero over the full $P_T^{J/\psi}$ range. It should be noted here that the fraction of directly produced J/ψ's in the prompt sample is approximately 64% as discussed in Section 3.

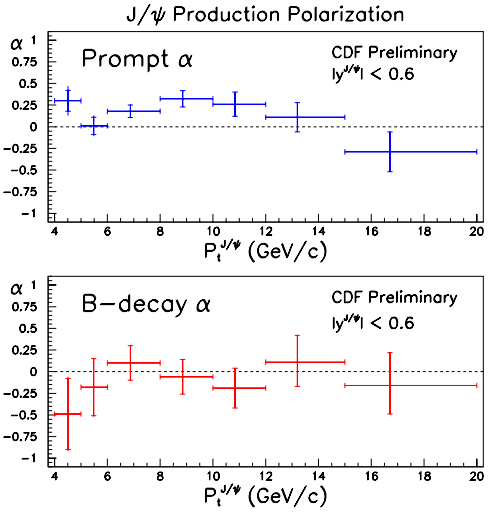

Figure 10: Fitted J/ψ polarizations for the prompt and B decay components in the $P_T^{J/\psi}$ range 4 to 20 GeV/c

5. Measurement of Production Polarization of ψ'

The data samples used in this study by CDF were dimuon triggers from Run I with an integrated luminosity of 110 pb^{-1}. Both muons were required to be measured in the SVX detector and the P_T of the dimuon system was required to be above 5.5 GeV/c. Figure 11 shows the dimuon mass spectrum from 3.45 to 3.9 GeV/c^2 which shows a clear peak of 1776 ± 62 signal ψ' events. In a 3σ mass window around the ψ' mass the signal to background ratio is 1.05 ± 0.04.

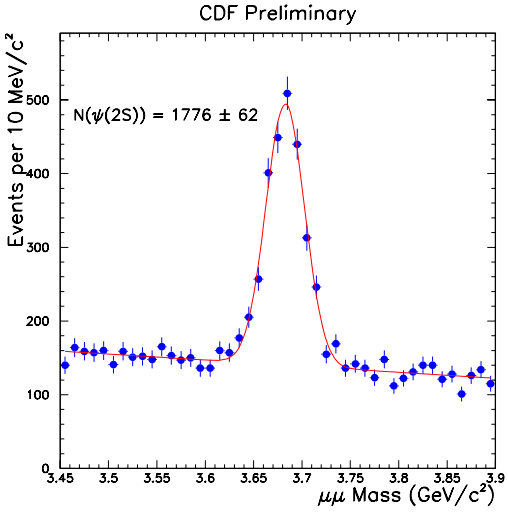

Figure 11: ψ' mass distribution. The fit is a Gaussian with a linear background.

The data were divided into 3 P_T bins and 2 subsamples based on the ψ' ct distribution. The low ct region $-0.1 \leq ct \leq 0.01$ cm is prompt enriched whereas the high ct region $0.01 \leq ct \leq 0.3$ cm is dominated by B decays. The numbers of events as a function of $|cos\theta|$ are obtained by fitting the mass distributions with a Gaussian and a linear background. In each subsample the $|cos\theta|$ distribution was fitted to a sum of 2 angular distributions with parameters α^P and α^B corresponding to prompt and B decay production respectively. The relative fraction of each distribution was known from the fits to the ct distributions. An example of the fitted angular distributions obtained are shown in Figure 12 for the prompt enriched sample for the 3 $P_T^{\psi'}$ ranges 5.5-7, 7-9, 9-20 GeV/c and the combined sample 5.5-20 GeV/c respectively.

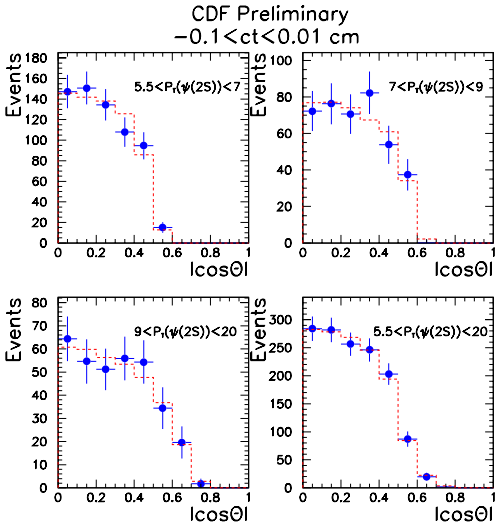

Figure 12: The fitted $|cos\theta|$ distributions for the prompt enriched region

Figure 13 shows the fitted values of α^P as a function of $P_T^{\psi'}$ in the range 5.5 to 20 GeV/c. The curve is the expected polarization from the COM [12] which is seen to be above the data at high P_T but only by 2 standard deviations.

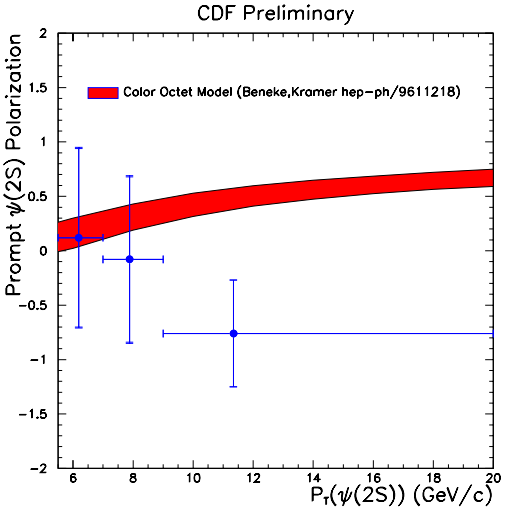

Figure 13: The fitted ψ' polarizations for the prompt component in the $P_T^{\psi'}$ range 5.5 to 20 GeV/c. The curve is the expected polarization from the COM [12]

Figure 14 shows the fitted values of α^B as a function of $P_T^{\psi'}$ in the range 5.5 to 20 GeV/c. Here there are no predictions by theory but the data have large statistical errors and no clear statement is possible.

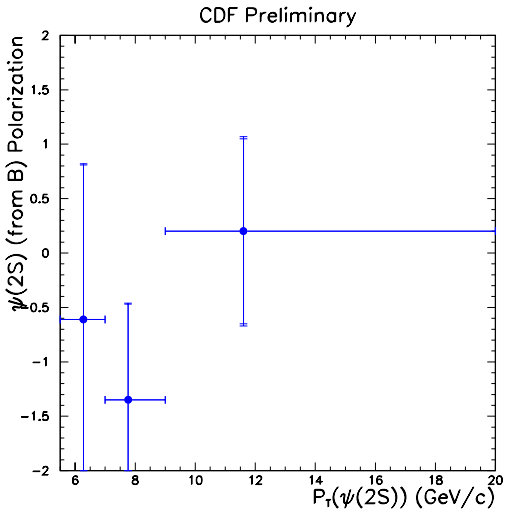

Figure 14: The fitted ψ' polarizations for the B decay component in the $P_T^{\psi'}$ range 5.5 to 20 GeV/c.

the systematic errors added in quadrature. Figures 17 and 18 show the differential cross sections for the $\Upsilon(2S)$ and $\Upsilon(3S)$ respectively. For these cross sections an additional systematic error has been computed by varing the production polarization using transverse and longitudinal Monte Carlo samples. This error is found to be less than the statistical error. Again, the error bars represent the statistical error plus the systematic errors added in quadrature. All three differential cross sections have a similar shape with a turn over at small P_T consistant with the production of a heavy meson. Figure 19 shows each differential cross normalised by its own cross section plotted on one graph. There is a slight indication that the $\Upsilon(2S)$ and $\Upsilon(3S)$ differential cross sections are stiffer at higher P_T than that of the $\Upsilon(1S)$.

In section 3 we showed that CDF has measured the relative fractions of directly produced J/ψ's, prompt J/ψ's from χ_c decays and ψ''s and J/ψ's from B decays. For $\Upsilon(1)$ production there will be contributions from higher mass Υ states and χ_b decays.

6. Υ Production Measurements

CDF has previously published results on Υ production based on 16.6 pb^{-1} of dimuon triggers [13]. Preliminary measurements based on ∼77 pb^{-1} of dimuon trigger data collected during Run Ib are presented here. Figure 15 shows the dimuon mass spectrum from 8.8 to 11.2 GeV/c^2 and the peaks for the $\Upsilon(1S)$, $\Upsilon(2S)$ and $\Upsilon(3S)$ are clearly visible. The number of events in each peak is obtained by fitting the distribution to a sum of Gaussians and a quadratic background.

This mass distribution is then fitted as a function of the dimuon P_T in order to extract the differential cross sections. Account is taken of the change in mass resolution and the detector acceptance as function of P_T using a Monte Carlo. Figure 16 shows the resulting $\Upsilon(1S)$ differential cross section. The Monte Carlo correction assumes that the $\Upsilon(1S)$ is produced unpolarized. This assumption is shown to be justified below. The error bars represent the statistical error plus

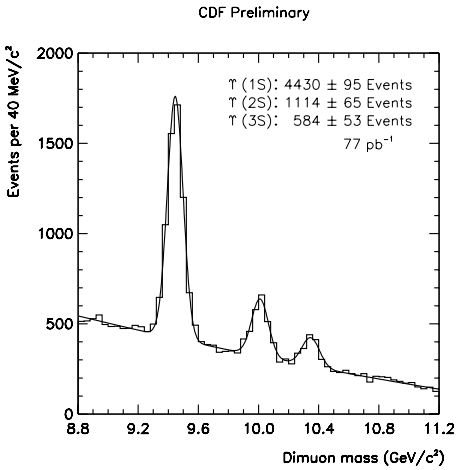

Figure 15: The dimuon invariant mass distribution in the Υ mass region.

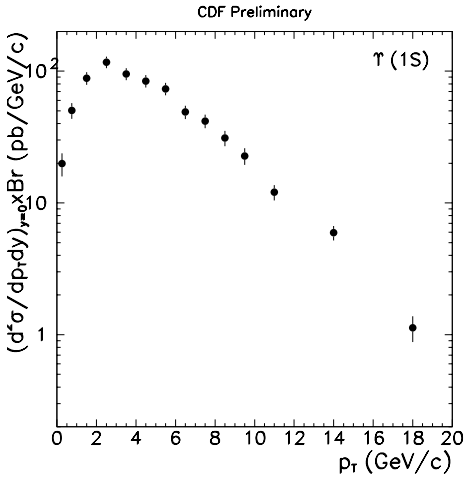

Figure 16: The differential cross section times $\mathrm{Br}(\Upsilon \to \mu^+\mu^-)$ for $\Upsilon(1S)$ production.

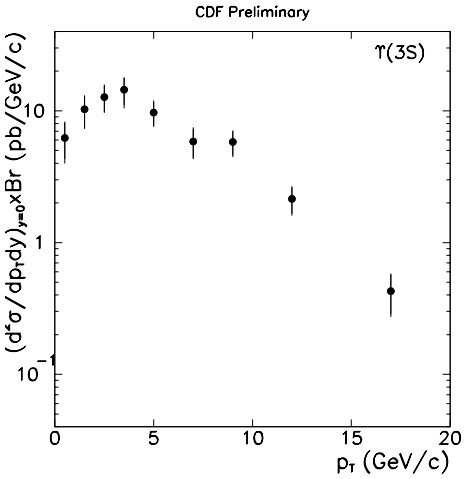

Figure 18: The differential cross section times $\mathrm{Br}(\Upsilon \to \mu^+\mu^-)$ for $\Upsilon(3S)$ production.

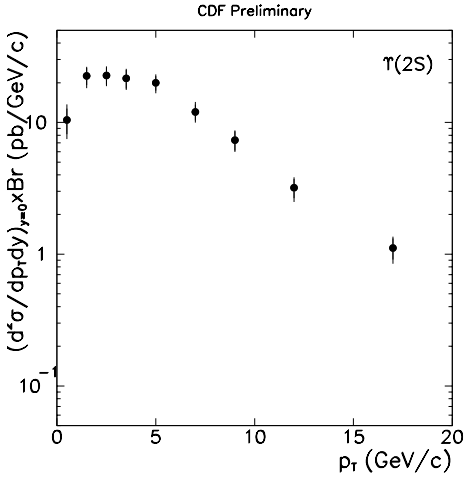

Figure 17: The differential cross section times $\mathrm{Br}(\Upsilon \to \mu^+\mu^-)$ for $\Upsilon(2S)$ production.

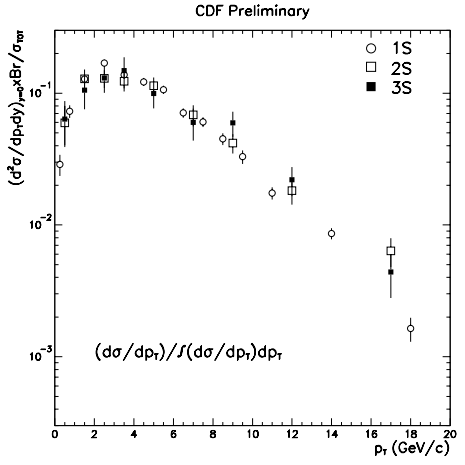

Figure 19: The normalised differential cross sections for $\Upsilon(1S)$, $\Upsilon(2S)$ and $\Upsilon(3S)$.

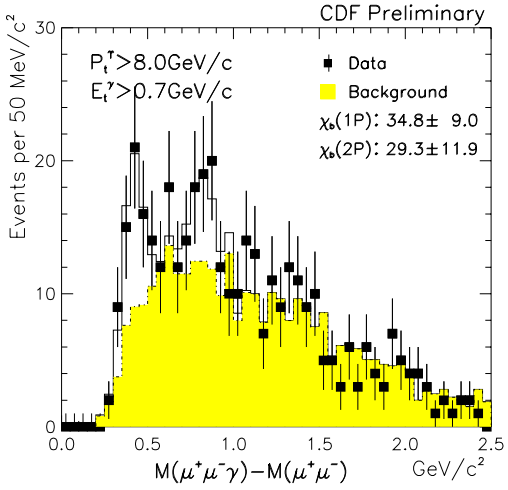

Figure 20: The mass difference $\Delta M = M(\mu^+\mu^-\gamma) - M(\mu^+\mu^-)$ for $P_T^\Upsilon > 8.0$ GeV/c and photon candidates above 0.7 GeV.

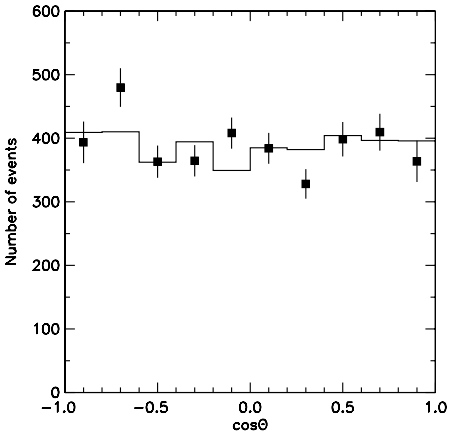

Figure 21: Fitted background subtracted $cos\theta$ distribution for the $\Upsilon(1S)$ in the range $2 < P_T^\Upsilon < 20$ GeV/c.

CDF has searched for the radiative decays of χ_b and see evidence for $\chi_b(1P) \to \Upsilon(1S)\gamma$ and $\chi_b(2P) \to \Upsilon(1S)\gamma$ at relatively high P_T. Photon candidates above 0.7 GeV are combined with dimuons in the $\Upsilon(1S)$ signal region with $P_T^\Upsilon > 8.0$ GeV/c. Figure 20 shows the mass difference $\Delta M = M(\mu^+\mu^-\gamma) - M(\mu^+\mu^-)$. The background shape is obtained from a Monte Carlo that uses real $\Upsilon(1S)$ as input and generates photons from charged tracks in the event assuming them to be π^0, η or K_s in an appropriate ratio. Two peaks above background associated with the decays $\chi_b(1P) \to \Upsilon(1S)\gamma$ and $\chi_b(2P) \to \Upsilon(1S)\gamma$ are seen. From these peaks the fractions of $\Upsilon(1S)$ with $P_T^\Upsilon > 8.0$ GeV/c are determined to be $(26.7\pm 6.9 \pm 4.3)\%$ and $(10.8 \pm 4.4 \pm 1.3)\%$ respectively.

A simulation of the decays $\Upsilon(2S) \to \Upsilon(1S)\pi\pi$ gives the fraction of $\Upsilon(1S)$ with $P_T^\Upsilon > 8.0$ GeV/c from $\Upsilon(2S)$ as $(10.7 \pm 2.5 \pm^{+7.4}_{-4.3})\%$. The contribution from $\Upsilon(3S)$ is assumed to be negligible. Subtracting the contribution from χ_b's and Υ's the fraction of directly produced $\Upsilon(1S)$'s is found to be $(51.8 \pm 8.2 \pm^{+9.0}_{-6.7})\%$ for $P_T^\Upsilon > 8.0$ GeV/c.

CDF has performed a polarization analysis on the $\Upsilon(1S)$ data in a similar manner to that on the J/ψ without the complication of separating the prompt and B decays. All Υ's are produced promptly and it is not possible to separate out the directly produced decays. The $cos\theta$ distribution for $|y_\Upsilon| < 0.4$ and $2 < P_T^\Upsilon < 20$ GeV/c is shown in figure 21.

The angular distribution is not as truncated by the acceptance at large $|cos\theta|$ because of the high mass of the Υ relative to the P_T cuts on the decaying muons. In this case the longitudinal fraction Γ_L/Γ is measured to be (0.37 ± 0.04). This is given in terms of the usual polarization parameter α as $\Gamma_L/\Gamma = (1-\alpha)/(3+\alpha)$ from which $\alpha = -0.08 \pm 0.09$ is calculated. Restricting the P_T^Υ to be in the range $8 < P_T^\Upsilon < 20$ GeV/c yields a value of $\Gamma_L/\Gamma = 0.32 \pm 0.11$ which corresponds to a value of $\alpha = 0.03 \pm 0.25$. Hence the Υ is unpolarized also at the higher values of the P_T^Υ. This result probably does not contradict the predictions of the COM as transverse polarization is only expected to be large at transverse momenta P_T for $P_T^2 \gg m_q^2$ where m_q in this case is the b quark mass [12].

References

[1] F. Abe *et al.,Phys. Rev. Lett.* **71** (1993) 500; F. Abe *et al.,Phys. Rev. Lett.* **71** (1993) 2396.

[2] S. Abachi *et al.,Phys. Rev. Lett.* **74** (1995) 3548; S. Abachi *et al.,Phys. Lett.* **B 370** (1996) 239.

[3] P. Nason, S. Dawson and R.K. Ellis, *Nucl. Phys.* **B 327** (1989) 49.

[4] M. Mangano, P. Nason and G. Ridolfi, *Nucl. Phys.* **B 373** (1992) 295.

[5] C. Albjar *et al.,Z. Physik* **C 61** (1994) 41.

[6] F. Abe *et al.,Phys. Rev.* **D 53** (1996) 1051.

[7] F. Abe *et al.,Phys. Rev. Lett.* **79** (1997) 572

[8] E. Braaten, M.A. Doncheski, S. Fleming and M.L. Mangano, *Phys. Rev. Lett.* **333** (1994) 548; M. Cacciari and M. Greco, *Phys. Rev. Lett.* **73** (1994) 1586.

[9] F. Abe *et al.,Phys. Rev. Lett.* **79** (1997) 578

[10] G.T. Bodwin *et al.,*, *Phys. Rev.* **D 46** (1992) R3703

[11] E. Braaten and S. Flemimg, *Phys. Rev. Lett.* **74** (1995) 3327; P. Cho and M. Wise, *Phys. Lett.* **B 346** (1995) 129; M. Cacciari, M. Greco, M.L. Mangano and A. Petrelli, *Phys. Lett.* **B 356** (1995) 553; P. Cho and A.K. Leibovich, *Phys. Rev.* **D 53** (1996) 150; P. Cho and A. K. Leibovich, *Phys. Rev.* **D 53** (1996) 6203.

[12] P. Cho and M. Wise, *Phys. Lett.* **B 346** (1995) 129; M. Beneke and M. Kramer, *Phys. Rev.* **D 55** (1997) 5269.

[13] F. Abe *et al.,Phys. Rev. Lett.* **75** (1995) 4358.